JOURNAL OF MATERIALS SCIENCE 29 (1994) 3071–3079

Effect of notch severity on fatigue fracture in a rubber-modified glassy polymer

M. RINK, B. GUIDETTI, R. FRASSINE
Dipartimento di Chimica Industriale e Ingegneria Chimica-Politecnico di Milano, Piazza Leonardo da Vinci 32, 20133 Milano, Italy

L. CASTELLANI
ECP Enichem Polimeri, Via G. Taliercio 14, 46100 Mantova, Italy

The research concerned the effect of notch severity on the fatigue behaviour of series of rubber-modified glassy polymers, consisting of a styrene–acrylonitrile copolymer with different amounts of an olefin rubber. Tests were conducted under displacement control and two different loading conditions. Both stages of fatigue lifetimes, that is, fracture initiation and crack propagation, were examined. It was observed that the initial notch severity determines the duration of the crack-initiation stage, while crack propagation does not depend on it. The crack velocity appears to be controlled by the maximum applied stress intensity factor, and the correlation does not depend on the rubber content. The results obtained have been interpreted by considering three different zones in the specimen during the fracture process: a far-field viscoelastic continuum, a process zone and a failure zone.

1. Introduction

Material optimization for fatigue fracture resistance is a difficult task because of the large number and variety of material and test variables that may play a role in determining this property. In the case of rubber-modified glassy polymers, results in the literature are often contradictory. Positive and negative [1–8] effects of the addition of rubber to glassy polymers have both been reported. Different effects of rubber modification on the two stages of fatigue failure (crack initiation and crack propagation) have been suggested because inconsistent results have been obtained in tests on unnotched specimens in which the initiation stage is predominant, compared with results obtained on notched specimens. Even in tests using sharply notched specimens, a large part of the fatigue lifetime may be due to the initiation stage [9]. For a better understanding of the role played by the dispersed rubbery phase and by the severity of the initial notch in both stages of fatigue fracture, we performed fatigue tests on a series of rubber-modified styrene–acrylonitrile copolymers, using notched specimens with different radii at the tip of the notch.

1.1. Materials

An olefin-rubber-modified styrene–acrylonitrile copolymer (AES), produced by EniChem Polimeri, was used for this work. The base material (AES 40) consisted of a continuous styrene–acrylonitrile (SAN) matrix in which approximately spherical rubber particles were dispersed.

Samples with different rubber contents, labelled as AES 5, AES 15, AES 25, were obtained by diluting (via extrusion blending) the same batch (AES 40) with different amounts of a SAN copolymer (named AES 0) with a molecular-weight distribution and an acrylonitrile (AN) content close to those of the matrix of the starting batch.

In order to check the possible effect of the molecular weight of the SAN matrix, a sample, AES B15, was prepared from a different batch by blending it with a higher-molecular-weight SAN. The resulting structural data are shown in Table I. The rubber-phase contents were measured by separation with selective solvents; number-averaged (M_n) and weight-averaged (M_w) molecular weights of the continuous phases were measured by gel-permeation chromatography. All SAN phases were found to have the same AN content (24% by weight), on determination by infrared spectroscopy.

An approximate evaluation of the rubber-particle-size distribution was obtained by determining the statistical distribution of particle section diameters observed in transmission electron microscopy (TEM) images; average diameter values are listed in Table I. The rubber particle size of AES B15 turned out to be slightly higher than that of the other samples.

A TEM micrograph of sample AES 40, which is representative of the general morphology of the materials investigated, is shown in Fig. 1.

2. Experimental details

2.1. Basic mechanical properties

The tensile modulus and yield stress of the materials were determined at room temperature on dumbell specimens of 50 mm gauge length, by performing

0022–2461

TABLE I The main structural characteristics of the samples (see text)

Sample	Rubber content (wt %)	Particle size (μm)	SAN matrix	
			(M_w)	(M_w/M_n)
AES 0	0	–	95 600	1.73
AES 5	5.8	–	92 700	1.75
AES 15	15	0.16	92 800	1.76
AES 25	24.1	0.14	89 140	1.75
AES 40	39.4	0.16	91 520	1.74
AES B15	15.8	0.22	126 000	2.07

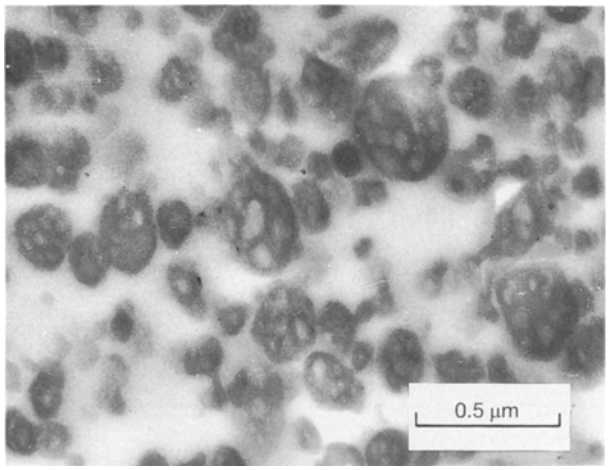

Figure 1 Transmission electron micrograph of the AES 40 material.

tensile tests at a constant displacement rate of 5 mm min^{-1}, with an Instron dynamometer.

2.2. Fracture under monotonic loading

The J-integral was determined by three-point bending, SE(B), on sharply notched specimens with dimensions of $6 \times 12 \times 65$ mm^3, following the procedure given in [10].

2.3. Fatigue-fracture tests

The test configuration was single edge-notch tension, SE(T), with bending restrained. Specimens had dimensions of $110 \times 23 \times 3$ mm^3, notched on the longest edge. Notches with five different tip radii (0.009, 0.09, 0.15, 0.19 and 1 mm) were introduced by sliding different blades into the material. All initial notches were 1 mm long.

Tests were performed on samples AES 15, AES 25 and AES 40, at 23 °C on an Instron servo-hydraulic machine, by applying a sinusoidal displacement at a frequency of 1 Hz. Two different loading conditions, both with the same ratio (1/3) between the minimum and the maximum displacement, were considered. In the first condition, the same tensile displacement of 0.9 $\pm$ 0.45 mm was applied to the different materials, and the ratio between the maximum applied stress at the beginning of the test, σ^0_{max}, and the yield stress, σ_y, turned out to be about 0.6 for all materials. Under such a condition, yield zones of similar sizes were expected to develop at the tip of similar cracks in different materials. In the second condition, different displacements were applied to the different materials so as to produce the same initial value of 18 MPa of the applied stress, σ^0_{max}. With the AES 40 sample, the two loading conditions coincided.

During the tests, crack growth was monitored by means of a video-recording system. Both fracture stages, fracture crack initiation (FCI) and fracture crack propagation (FCP), were considered.

A value of the maximum applied stress intensity factor, K_{max}, was calculated during the propagation stage by use of the linear elastic fracture mechanics relationship

$$K_{max} = \sigma_{max} Y a^{1/2}$$

in which Y is a factor depending on the specimen geometry adopted (this was experimentally determined previously for this test configuration [9]) and σ_{max} is the maximum applied stress (varying with time and crack length, a, under the displacement control used here).

Although an elasto-plastic-fracture-mechanics approach would probably have been more appropriate for this material, the linear elastic stress intensity factor was preferred in view of its simplicity, and it has proved to be a sufficiently good parameter for correlation with the crack-propagation rate for our purposes.

3. Results

3.1. Basic mechanical properties

Fig. 2 shows the tensile modulus, E, and the yield strength, σ_y, as a function of the rubber content for all the materials presented in Table I. Both quantities, as expected, decreased as the rubber content increased. Values for the material AES B15 did not differ appreciably from those of material AES 15 with approximately the same rubber content but different molecular weight (MW) molecular-weight distribution (MWD).

3.2. Fracture resistance under monotonic loading

Fig. 3 gives the values of the fracture resistance at crack initiation, J_{Ic}, as a function of the rubber content for all the materials examined. J_{Ic} increased with the rubber content up to about 25% rubber and then remained constant with further increases in the rubber content. The fracture resistance of the material AES B15 was considerably higher than that of AES 15, evidencing the important role of the molecular characteristics of the SAN matrix as regards fracture properties.

3.3. Fatigue fracture

3.3.1. Phenomenology observed

The effect of the notch-tip radius on the fatigue behaviour of the different materials was studied by conducting tests in the two different loading conditions

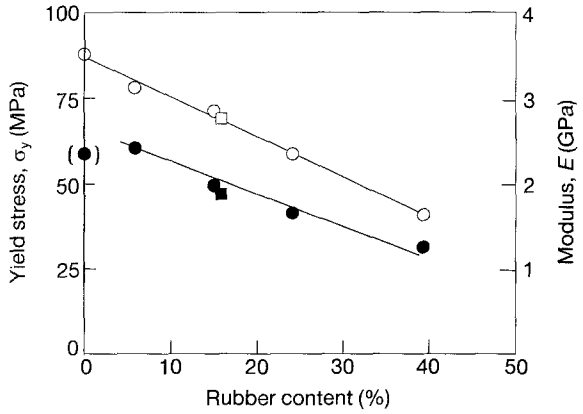

Figure 2 Tensile yield stress and modulus as a function of the rubber content. (○, ●) AES 0–40 modulus and yield stress respectively. (□, ■) AES B15, modulus and yield stress respectively. Value in brackets fracture stress.

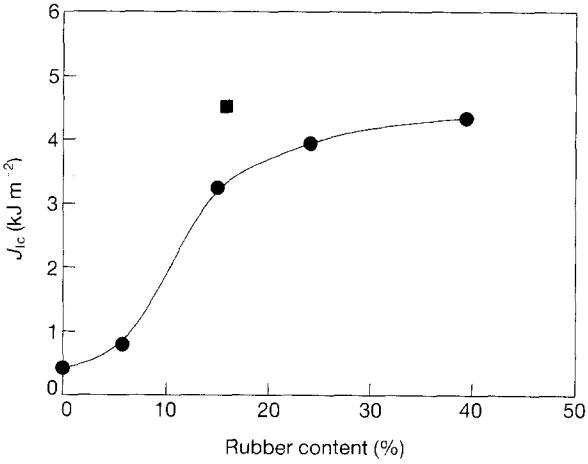

Figure 3 Fracture toughness, J_{Ic}, as a function of the rubber content: (●) AES 0–40, (■) AES B15.

described above. For each test performed, the maximum stress, σ_{max}, and the crack length, a, were recorded as a function of the number of loading cycles. Figs 4, 5 and 6 show significant examples of the plots obtained, together with photographs taken during the test. From these diagrams, two distinct phases of fatigue life could be identified. An initiation phase (lasting N_i cycles) during which the crack does not advance; but, as a consequence of the far-field viscoelastic behaviour of the material and of local yielding at the crack tip, overall stress relaxation occurs. The initiation was followed by a propagation stage (lasting N_p cycles), during which the crack advanced and a more rapid decrease in stress was observed, until the specimens finally broke. The propagation stage was observed to take place in three different modes, depending on the loading conditions, the notch type and the material characteristics.

3.3.1.1. Continuous crack propagation (Type I). The crack length increased at each cycle. An example of this type of behaviour is shown in Fig. 4. A small crack jump was first observed, after which the crack advanced regularly as cycling proceeded. Photographs of

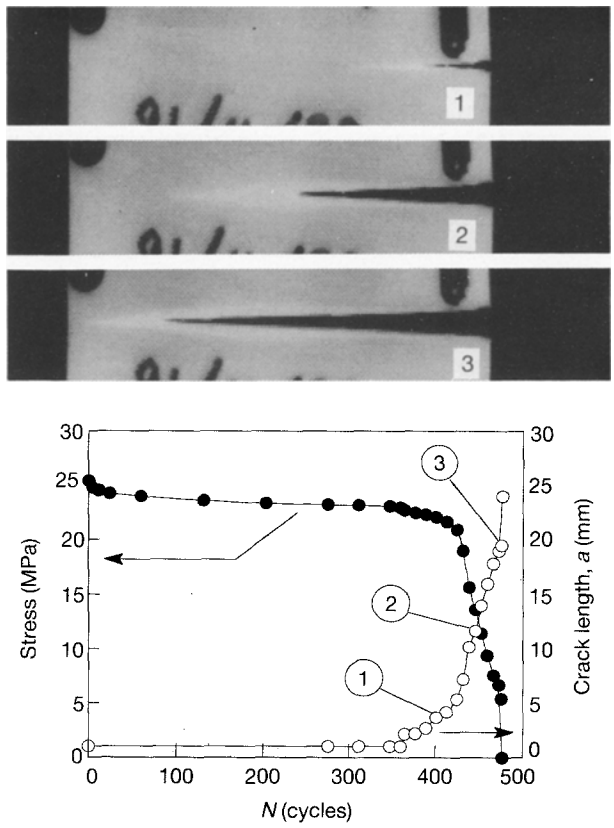

Figure 4 The maximum stress and crack length as a function of the number of cycles in the case of continuous crack propagation (for AES 25, with a notch radius of 9 μm, first loading condition). The numbers on the graph correspond to the numbered photographs of the lateral surface of the specimen during the test. ((●) stress, (○) crack length).

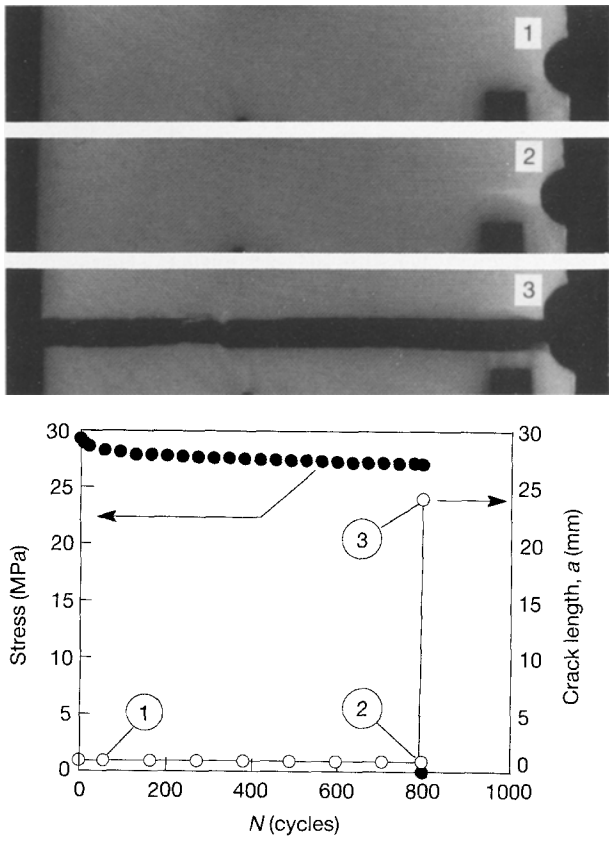

Figure 5 The maximum stress and crack length as a function of the number of cycles in the case of catastrophic crack propagation (for AES 15, with a notch radius of 1 mm, first loading condition). The numbers on the graph correspond to the numbered photographs of the lateral surface of the specimen during the test.

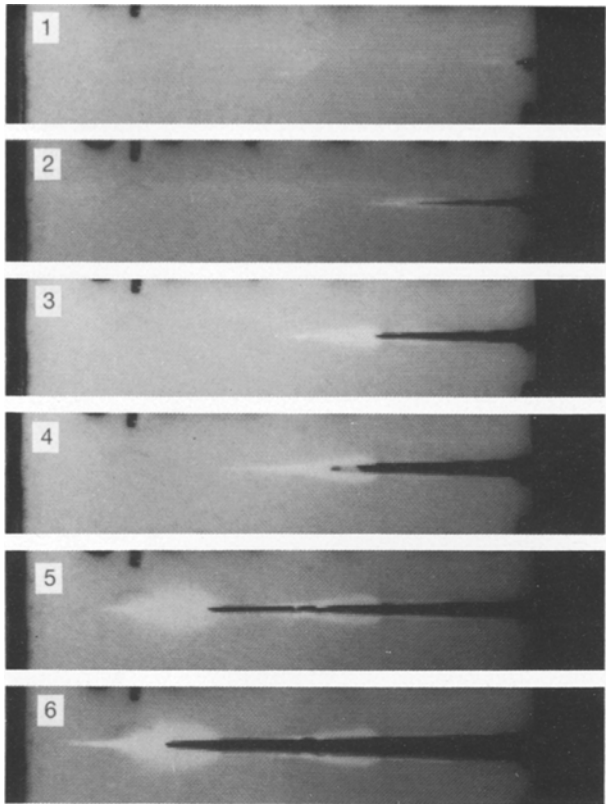

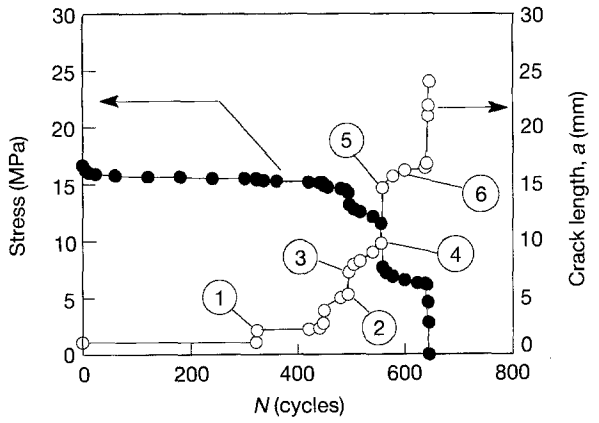

Figure 6 The maximum stress and crack length as a function of the number of cycles in the case of discontinuous crack propagation (for AES 40, with a notch radius of 9 μm). The numbers on the graph correspond to the numbered photographs of the lateral surface of the specimen during the test.

the specimen, taken at different stages of crack propagation during the test, show a slender, cusp-shaped whitened area ahead of the crack tip, which reveals that the fracture process zone was very localized along the crack-propagation path.

3.3.1.2. Catastrophic crack propagation (Type II). The crack advanced through the whole ligament in one cycle. Fig. 5 shows an example of this type of behaviour. From observation of the lateral surface of the specimen during the test, only a very small whitened area ahead of the crack tip can be noticed in this case.

3.3.1.3. Discontinuous crack propagation (Type III). In this case, the crack propagated in jumps, alternating with stages during which continuous stable crack growth (some advance at each cycle) occurred. An example of this type of behaviour is given in Fig. 6, and line drawings of the specimen surface at different stages of crack propagation are shown in Fig. 7: Fig. 7a and c were taken immediately after a jump, while Fig. 7b and d were taken at the end of the subsequent continuous growth. It may be observed that a very complex whitened area developed ahead of the crack tip during each jump, until the crack came to a complete stop Fig. 7a and c. This area can be divided into two distinct zones. The outer portion is less whitened, and it has two symmetrical branches that depart from the fracture plane at an angle of about 35°. The inner portion is more whitened, and can be thought of as the superposition of an ellipsoid on a cusp-shaped area. During the subsequent slow-crack-propagation stage, the crack moved across the existing whitened zone together with the cusp-shaped portion of the whitened area, as was observed in the case of Type-I propagation. When the crack tip reached the boundaries of the original whitened area (Fig. 7b and d) a new jump occurred.

3.3.2. Effect of the notch severity and the material

The effect of the notch severity on the fatigue behaviour of materials with different rubber contents (that is AES 15, 25 and 40) and different molecular-weight

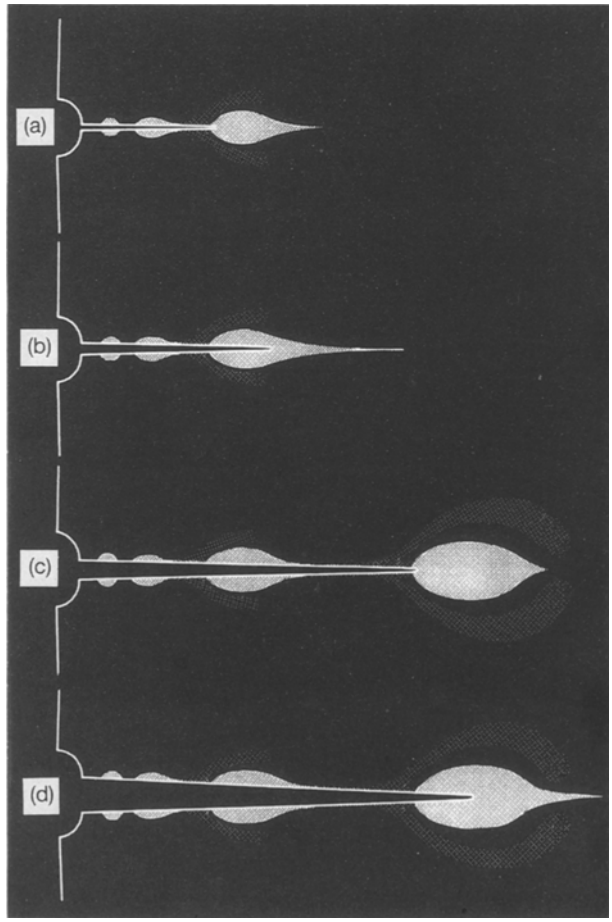

Figure 7 Line drawings of the specimen surface at different stages of crack propagation.

distributions (that is, AES 15 and AES B15) will be presented separately for each loading condition.

3.3.2.1. Same maximum applied displacement. Fig. 8 shows the trends of the number of cycles to failure, N_t, to fracture initiation, N_i, and to crack propagation, N_p, as a function of the notch-tip radius, ρ, for the first loading condition (corresponding to the same displacement for all the materials) for the three materials, AES 15, 25 and 40. The material AES 40 displayed discontinuous crack propagation (Type III) for all the notch radii examined.

The other two samples (with rubber contents of 15 and 25%) showed continuous crack propagation (Type I) for notch radii below a certain value, while above this value catastrophic propagation (Type II) was observed. The notch-tip radius at which the transition from continuous to catastrophic fracture occurred was higher for higher rubber contents (Figure 8c).

The total number of cycles to failure, N_t, increased with the notch-tip radius, irrespective of the different crack-propagation type observed (Fig. 8a). It can be further observed that the duration of the propagation stage, N_p, when not vanishing, did not seem to depend on the notch-tip radius (Fig. 8c); therefore, the increase in N_t caused by increasing the notch-tip radius depended only on the increase in the duration of the initiation stage (Fig. 8b). The observed constancy of N_p was not necessarily expected, for the fracture behaviour of viscoelastic materials generally depends on the entire loading history preceding crack growth.

As for the effect of the rubber content, N_t and N_i (and also N_p when crack propagation was not catastrophic) increased with the rubber content, irrespective of the notch sharpness.

Fig. 9 shows FCP-rate data for AES 15, AES 25 and AES 40, for all the different starting notches. Since AES 40 always exhibited discontinuous crack propagation under the applied test conditions, and as crack lengths cannot be measured accurately during crack jumps, the fracture mechanics approach was only applied in this case to the continuous-propagation stage between crack jumps. A single curve was obtained, indicating that the FCP behaviour was neither influenced by the different starting notches nor by the different rubber contents for these three materials. A similar dependence of the FCP rate on the rubber content was also observed by Bucknall and co-workers [11] on ABS resins under different loading conditions. A second series of tests was conducted on AES B15 with the same rubber content as AES 15, but a different MWD of the SAN matrix (see Table I). This

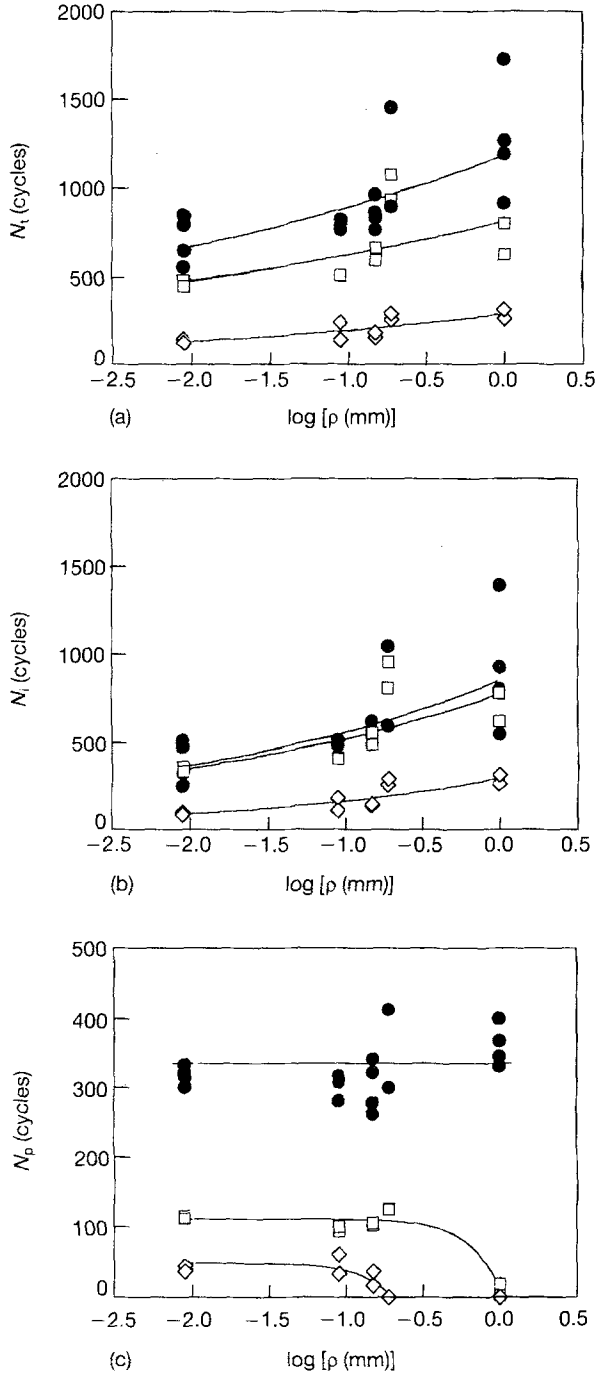

Figure 8 Number of cycles to (a) failure, N_t, (b) to fracture initiation, N_i, and (c) to crack propagation, N_p, as a function of the notch-tip radius, ρ, with varying rubber contents: (–◇–) AES 15, (–□–) AES 25, and (–●–) AES 40. Loading condition: same maximum applied displacement for all the materials.

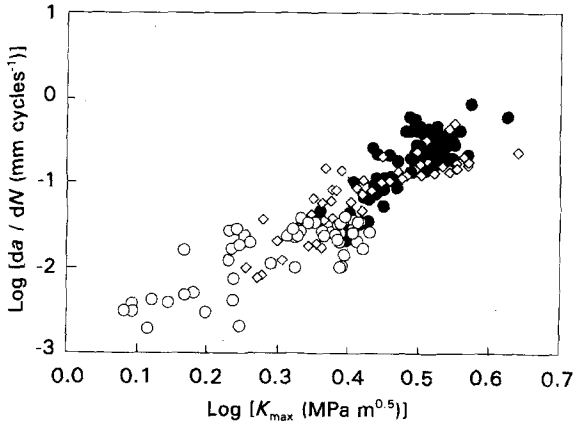

Figure 9 Fatigue-crack-propagation-rate graph for (◇) AES 15, (●) AES 25 and (○) AES 40 for all the notch radii examined. Loading condition: same maximum applied displacement for all the materials.

material showed the same type of phenomenology as that observed in AES 15, although the total lifetime increased (Fig. 10a). This increase is due to the increase in the number of cycles to crack initiation (Fig. 10b), while the propagation stage (Fig. 10c) does not seem to depend on the matrix MWD.

3.3.2.2. Same initial applied stress. Fig. 11 shows the trends of the number of cycles to failure, N_t, to fracture initiation, N_i, and to crack propagation, N_p, as a function of the notch-tip radius, ρ, for the second loading condition (corresponding to the same initial applied stress for all materials). This condition coincides with the first condition for the material AES 40, which, as already reported, displayed discontinuous crack propagation (Type III) for all the notch radii examined. The material AES 25 displayed continuous crack propagation for all the notch radii examined, and the material AES 15 showed continuous or catastrophic crack propagation in an apparently random way.

Although the data appeared to be more dispersed compared with the first loading condition (c.f. Fig. 8), the effect of the initial notch-tip radius on the fatigue

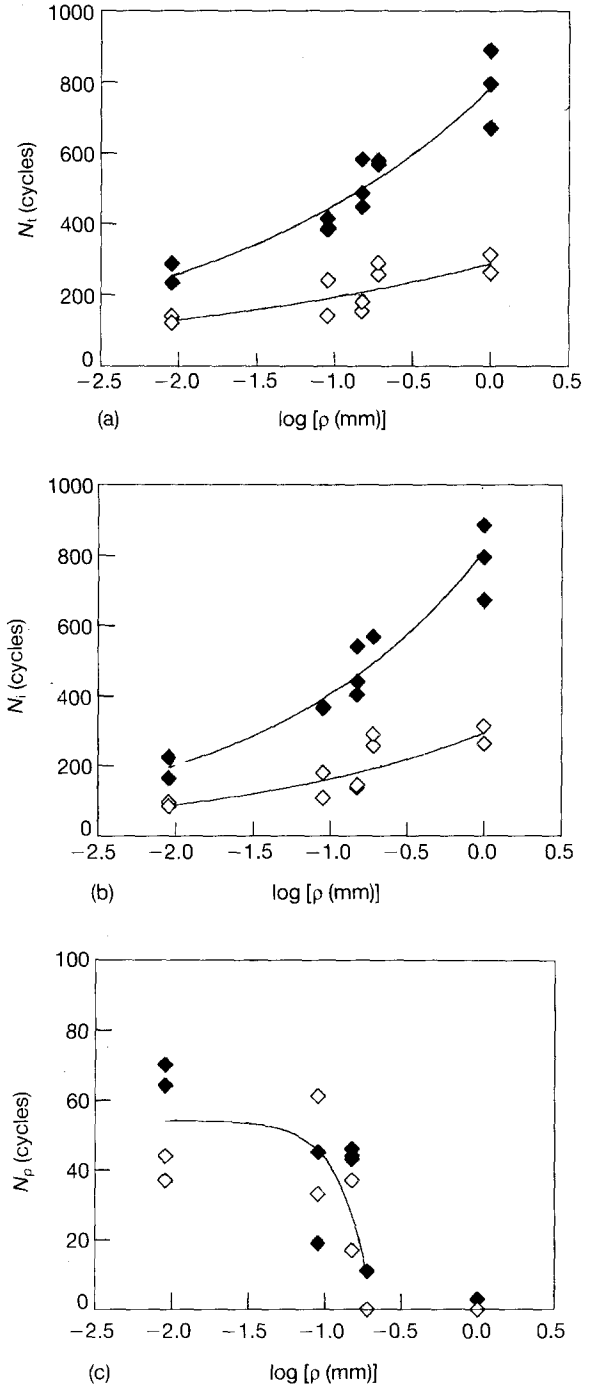

Figure 10 Number of cycles to (a) failure, N_t, (b) to fracture initiation, N_i, and (c) to crack propagation, N_p, as a function of the notch-tip radius, ρ, for materials with the same rubber content but different molecular-weight distributions of the SAN matrix (see Table I): (◇) AES 15, and (◆) AES B15. Loading condition same applied maximum displacement for both materials.

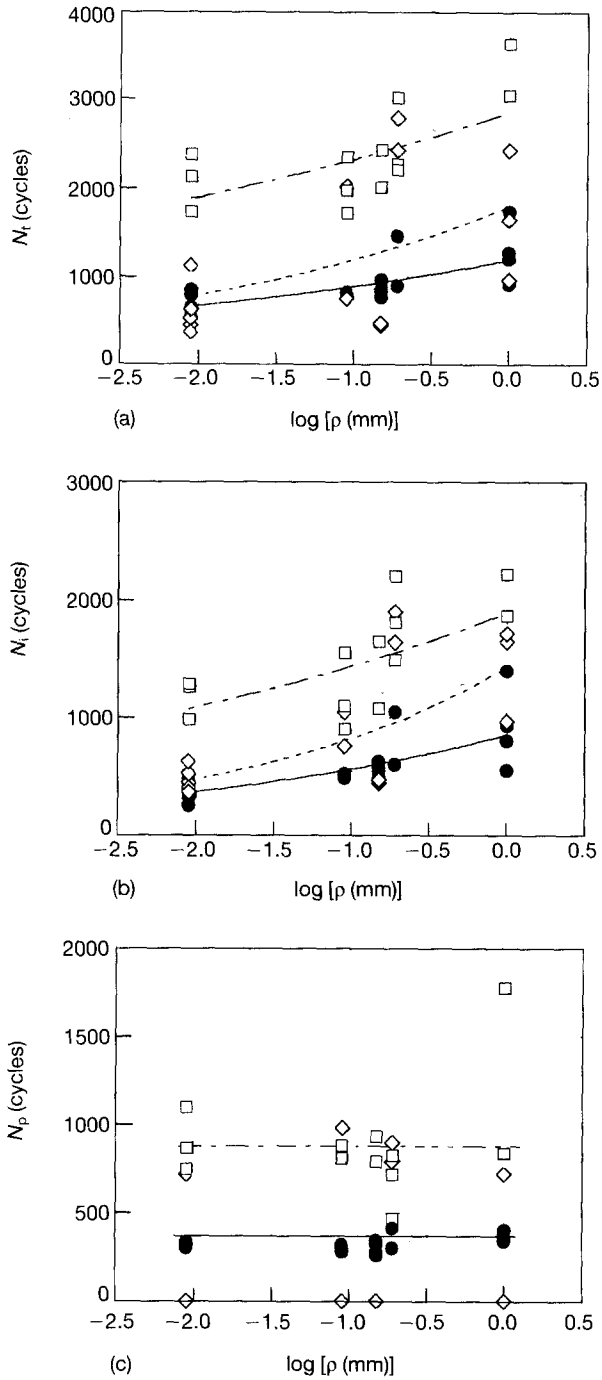

Figure 11 Number of cycles to (a) failure, N_t, (b) to fracture initiation, N_i, and (c) to crack propagation, N_p, as a function of the notch-tip radius, ρ, at varying rubber contents (- - - ◇ - - -) AES 15, (- - - □ - - -) AES 25, and (—●—) AES 40. Loading condition: same applied maximum displacement for all the materials.

lifetime is essentially the same. However, there appears to be maximum in the fatigue lifetime for rubber contents between 15 and 40%. The same materials were previously tested [9] for fatigue under load control, and they also showed the same non-monotonic trend in the fatigue lifetime with increasing rubber content.

Fig. 12 shows the fatigue-crack-propagation (FCP) rate da/dN, versus K_{max} for the material AES 25, based on data obtained from specimens with different starting notches, which showed stable crack propagation under the two loading conditions. All data occur on approximately the same line.

Thus, from the results in Figs 9 and 12, the maximum applied stress intensity factor appears to be the controlling parameter for the FCP rate of the materials examined, irrespective of the different starting notches considered, the loading condition or the rubber content.

4. Discussion

The objective of this research was to investigate the effect of notch severity on fatigue lifetime in a rubber-modified SAN matrix with varying rubber contents. The total fatigue lifetime was observed to increase regularly with the notch radius under both the loading conditions considered, as Figs 8a and 11a clearly show for the three rubber contents examined. With increasing rubber content, a progressive increase in the total fatigue lifetime was observed under the first loading condition (Fig. 8a), while, under the second loading condition, the maximum fatigue lifetime was observed for the intermediate rubber content (Fig. 11a).

For a possible interpretation of these results, three different zones should be considered in the sample during the fracture process: (i) the far-field viscoelastic continuum, in which the stresses are expected to relax with time at a certain rate, which will not be affected by the varying characteristics of the notch or the crack; (ii) the process zone, in which non-linear or yield phenomena occur due to the locally higher stress level ahead of the singularity; and (iii) the failure zone, which is relatively small volume of material contained inside the process zone, undergoing large deformations, in which material separation occurs.

Fracture is determined by the transfer of the external loading to the process zone through the viscoelastic far-field, by the stress intensification occurring at the singularity, which determines the size of the process zone, and by the intrinsic fracture resistance of the material inside the failure zone.

Some information on the contribution of the different factors mentioned above to the fracture process can be obtained from separate sets of experiments. For example, from dynamic-mechanical measurements on the materials studied, it may be deduced that the far-field viscoelastic effects at the temperature and frequency examined are probably determined by the glassy SAN matrix alone, irrespective of the different rubber contents; and it can also be determined that the possible hysteretic heating effects due to viscoelastic dissipation are very limited. Also, the fracture resistance, which obviously depends on the material, can be evaluated separately by more conventional fracture testing. Fig. 3 shows that, under monotonic loading at a constant strain rate, the fracture energy for crack initiation, J_{Ic}, increased with the rubber content up to about a 25% rubber, after which it levelled off.

To analyse the results of fatigue fracture here obtained, within the framework already described, it seemed best to consider the initiation stage (during which a crack develops, starting from the original machined notch) separately from the propagation stage (during which the crack may propagate by three different modes, as previously described).

4.1. Initiation stage

The number of cycles to initiate fracture, N_i, was observed to increase regularly as the notch severity decreased, that is, with increasing notch radius, under both of the loading conditions examined (Figs 8b and 11b). This result may not appear surprising since, by changing the notch radius, the far-field effects and the material resistance do not change, while the stress level ahead of the notch does. Because of the lower stress intensification produced by blunter notches, smaller process zones and longer initiation times may therefore be expected. The same type of correlation between notch severity and FCI was previously found for other materials [12].

The duration of the initiation stage, for a given notch, also depended on the rubber content. The same trend was observed for all the notch radii considered, and Fig. 13 shows, as an example, the number of cycles to initiation, N_i, as a function of the rubber content in the case of an initial notch radius of 9 μm.

Under the first loading condition (the circles in Fig. 13), N_i increased with the rubber content from 15 to 25%, and then with a further increase from 25 to 40% it remained approximately constant. Since the applied overall displacement was the same for the different materials in these experiments, the initial

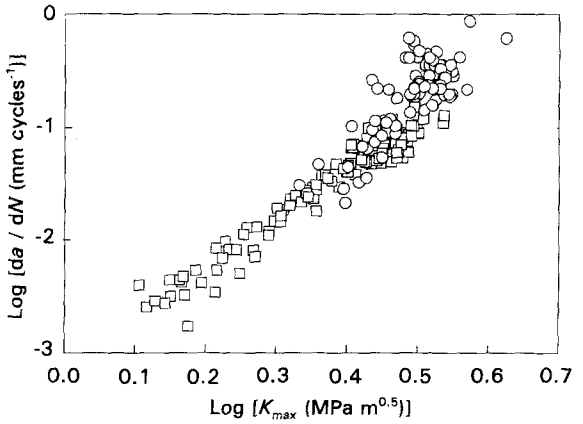

Figure 12 FCP-rate graph for the material AES 25 for all the notch radii examined: (○) same applied maximum initial stress, (□) same applied maximum displacement.

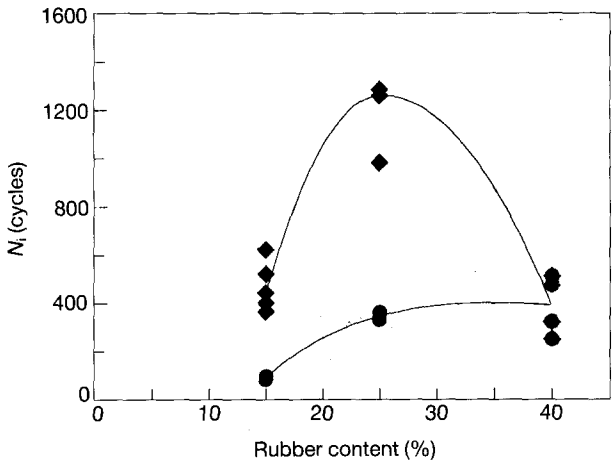

Figure 13 The number of cycles to fracture initiation, N_i, as a function of the rubber content under the two loading conditions considered. (●) the same applied maximum initial stress for all materials, (◆) the same applied maximum displacement for all materials. $\rho = 9$ μm.

stress applied decreased with increasing rubber content, paralleling the variation in the modulus, E, of the material (Fig. 2). Due to the decrease in the yield strength of the material as the rubber content increased, a fairly constant σ^0_{max}/σ_y ratio was then obtained for all the materials. This created process zones of similar sizes for the different materials. Therefore, the number of cycles to initiation was probably controlled, in this case, by the fracture processes acting inside the failure zone. In fact, N_i showed the same trend as the fracture energy, J_{Ic}, given in Fig. 3.

Under the second loading condition (the same σ^0_{max} for the different materials), as the rubber content increased, a maximum in N_i was observed (◆ in Fig. 13). If the fracture energy of the material alone had determined the initiation time, the same increase in N_i with rubber content as for the first loading condition should have been obtained. Now, however, as the rubber content increased so did the ratio σ^0_{max}/σ_y; this loading condition may therefore produce larger process zones and shorter initiation times. From these two distinct effects, with different trends, a non-monotonic dependence of N_i on the rubber content applies.

The FCI results obtained for AES B15 (Fig. 10b), when compared with those obtained for AES 15, confirm the above picture of the fracture process. Since the process-zone size is expected to be similar for both materials, σ_y and E being approximately the same (Fig. 2), the resistance of the material to crack initiation, J_{Ic}, was expected to play a major role in determining the initiation time. Therefore, the higher value of J_{Ic} shown in Fig. 3 for AES B15 appeared to be consistent with its larger number of cycles to initiation.

4.2. Propagation stage

Once a natural crack has been generated in the material ahead of the notch, the subsequent propagation stage may in principle depend on the original notch severity, on the loading conditions, and on the rubber content. When, at the end of the initiation stage, a natural crack starts to propagate, it moves into a stress field that differs according to the size of the existing process zone ahead of the notch. Process zones are generally assumed to be zones of yield material, which implies a redistribution of the local stress ahead of the notch. If the process-zone size is larger than the crack length critical for propagation (which may occur with sharper starting notches), and the crack speed is sufficiently slow to allow plasticization of the material ahead of the tip to take place during propagation, then cracks may propagate in a stable manner. On the other hand, if the process-zone size is smaller, or the crack speed is too high, the crack will experience a higher stress level ahead of its tip, and unstable crack propagation may ensue.

Fig. 8c reports data obtained under the first loading condition, showing that, for materials AES 15 and AES 25, crack propagation becomes catastrophic for notch radii above a certain value. This is consistent with the observation that the process-zone size decreased with the notch severity. Moreover, the transition from stable to catastrophic propagation occurred at a larger notch radius when the rubber content was increased from 15 to 25%. This result does not appear surprising considering that: (i) the process-zone size is similar for a given starting notch for different materials under this loading condition (the ratio σ^0_{max}/σ_y is the same); and (ii) the initial applied stress is higher for the material AES 15. Thus, a higher initial crack speed is in order for the material with the lower rubber content, and instability may be expected for sharper notches.

The type of propagation, irrespective of the starting notch radius, may be changed by changing the loading conditions. A comparison of Figs 8c and 11c shows that, for large-notch radii, a tendency for crack propagation to change from catastrophic to continuous propagation was observed for AES 15 and AES 25 when the loading condition was switched from the first loading condition (Fig. 8c) to the second (Fig. 11c). This change can be explained by observing that the initial stress, σ^0_{max}, is lower under the second loading condition, and that the crack-propagation velocity increased with the applied stress intensity factor (Figs 9 and 12).

The type of propagation also depended on the rubber content: under both loading conditions, AES 15 and AES 25 displayed continuous or catastrophic crack propagation, while AES 40 showed discontinuous crack propagation.

However, the duration of the propagation stage did not depend on the initial notch radius, at least within a single type of propagation (Figs 8c and 11c). This result follows from the data presented in Figs 9 and 12, which show that the crack-propagation rate is controlled by the applied stress intensity factor, irrespective of the starting notch radius.

The duration of the propagation stage as a function of the rubber content is shown in Fig. 14, containing data from tests with all the notch radii. Under the first loading condition, N_p regularly increased with the

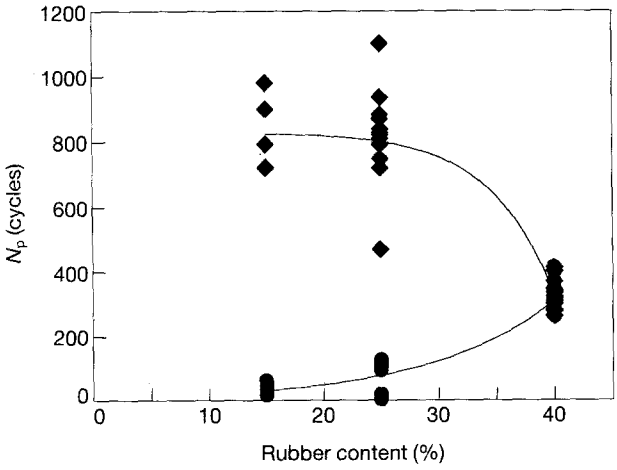

Figure 14 The number of cycles to fracture propagation, N_p, as a function of the rubber content under the two loading conditions. (●) the same applied maximum initial stress for all the materials; and (◆) the same applied maximum displacement for all the materials.

rubber content. This is due to the fact that, since the applied displacement is constant, the applied stress intensity factor, and thus the crack velocity, decreased by increasing the rubber content due to a decrease in the modulus, E. Under the second loading condition, since the applied overall stress is constant, the stress intensity factor applied during the test was approximately the same for all the materials. Cracks were thus expected to propagate at the same speed, leading to the same number of cycles, N_p. This is in fact the case for the two lower rubber contents (15 and 25%), which showed continuous crack propagation, while N_p for the material with 40% rubber content, which showed discontinuous crack propagation for all notch radii, was considerably lower than the previous values (Fig. 14). This is not surprising, since, for discontinuous propagation, the crack translates at a slow rate only for a limited length between each jump. The shortening of N_p for AES 40 is thus simply proportional to the jump number and size. Fig. 7 shows that the large process zone forming at each stop is able to control crack propagation, and some advance occurs at each cycle, until the crack tip reaches the boundaries of the process zone (frames b and d). In the next cycle, the slender failure zone that precedes the crack tip is not able by itself to lower the stresses sufficiently to prevent unstable crack propagation, and a new jump occurs. Discontinuous crack propagation can then be thought of as an behaviour intermediate between stable and unstable crack propagation.

To sum up, it is important to note that the number of cycles to propagation, N_p – propagation either takes place in a stable or discontinuous manner – may depend on the rubber content and/or the loading conditions, but it does not depend on the initial notch severity. It has also been shown that the rate of stable crack propagation depends on the applied stress intensity factor, irrespective of the rubber content – at least in the range explored. However, the transition from stable to unstable propagation, as well as the number of cycles to initiation, N_i, are strongly affected by the initial notch type. Finally, a transition from stable to discontinuous crack propagation was observed above a certain rubber content, which, in the case of a constant initial stress, produces a substantial shortening of the number of cycles to propagation.

Acknowledgements

The authors wish to thank Professor Andrea Pavan for valuable suggestions and discussions during the development of this work.

References

1. M. D. SKIBO, J. JANISZEWSKI, R. W. HERTZBERG and J. A. MANSON, in "Toughening of plastics I" (Plastics and Rubber Institute, London, 1978) p. 25.1.
2. DER-JIN WOAN, M. HABIBULLAH and J. A. SAUER, *Polymer* **22** (1981) 699.
3. J. A. SAUER and C. C. CHEN, *Polymer Engng. Sci.* **24** (1984) 786.
4. J. A. MANSON, R. W. HERTZBERG, M. J. CALING, M. T. HAHN, J. HWANG, J. TURKANIS and G. ATTALLA, in "Toughening of plastics II" (Plastics and Rubber Institute. London, 1985) p. 5.1.
5. J. A. SAUER and C. C. CHEN, *ibid.* (Plastics and Rubber Institute, London, 1985) p. 26.1.
6. J. L. TURKANIS, R. W. HERTZBERG and J. A MANSON, in "Deformation yield and fracture of polymers" (Plastics and Rubber Institute, Cambridge, 1985) p. 54.1.
7. C. C. CHEN and J. A. SAUER, *J. Appl. Polym. Sci.* **40** (1990) 503.
8. J. F. WANG, J. A. MANSON, R. W. HERTZBERG, G. A. MILLER and L. H. SPERLING, *Polym. Engng. Sci.* **29** (1989) 1477.
9. M. RINK, D. IMBRIGHI, L. CASTELLANI and A. PAVAN, in "ECF 8, fracture behaviour and design of materials and structures", edited by D. Firnao (EMAS Ltd, London, 1990) p. 201.
10. European Structural Integrity Society (ESIS), Technical Committee 4 "Polymers and composites", A Linear Elastic Fracture Mechanics (LEFM) Standard for Determining K_c and G_c for Plastics: Testing Protocol. March, 1990.
11. C. B. BUCKNALL and T. FAITROUNI, in "Deformation yield and fracture of polymers" (Plastics and Rubber Institute, Cambridge, 1991) p. 30.1.
12. A. BAUS, H. P. LIEURADE, G. SAUZ and M. TRUCHON, in "Flaw growth and fracture", ASTM STP 631 (American Society for Testing and Materials, Philadelphia, PA, 1977) p. 96.

Received 11 August 1992
and accepted 20 August 1993